COMSOL CONFERENCE 2023 MUNICH

Reinforcement bars corrosion in a carbonated concrete

Bruno Chinè[1], Ronald Jimenez S.[1], Rommel Cuevas K.[2]

1. School of Materials Science and Engineering, Costa Rica Institute of Technology, Cartago, Costa Rica.
2. School of Construction Engineering, Costa Rica Institute of Technology, Cartago, Costa Rica.

Abstract

In the construction sector, the concrete and the steel bars represent still the key components, although they are very vulnerable by the atmospheric agents, as in the case of their degradation caused by corrosion. The value of the concrete carbonation may enhance the corrosion around the reinforcing bar, promoting deterioration of the mechanical properties of the material and finally of the structure. In this work we present a computational model of the reinforcement corrosion in a carbonated concrete, based on experimental data obtained from a carbonation process and corrosion of the metallic bars. Using an accelerated carbonation chamber, we carried out testing on cylindrical concrete samples reinforced with four steel bars, followed by electrochemical measurements to characterize the corrosion mechanism of the metal elements. The experimental data are then introduced in Comsol Multiphysics® 6.1 to model the corrosion of the reinforcing metal under steady state conditions. We define the electrochemical mechanism of the bars using the Second Current Distribution of the Corrosion Module, while the computation of the oxygen diffusion is developed with the Transport of Dilute Species interface of the Chemical Reaction Engineering Module. The model is completed by incorporating experimental kinetics data of the electrochemical electrode reactions, reflecting the carbonation front progress. Starting from experimental values of corrosion potential, corrosion current density, anodic, and cathodic slopes of the Tafel curve, the values of exchange currents are computed and then used to simulate the corrosion of four reinforcing bars. According to the computational results, the outermost bars are characterized by stronger corrosion and reduction currents, phenomena depending also on the oxygen concentration values associated to the coupled gas diffusion process.

Keywords: concrete, carbonation, corrosion, exchange current density, computational modelling.

Introduction

Although concrete and metal reinforcement are very vulnerable to atmospheric agents, they represent the most widely used materials for civil constructions. Since the carbon dioxide is increasing in the atmosphere due to the climate change, it is necessary to evaluate the impact of corrosion on civil structure [1,2] for safety reasons and the high costs associated with their repair or replacement.

Concrete is fundamentally a porous ceramic material [3], with a structure exposed to atmospheric degradation mechanisms caused by carbonation. When CO_2 diffuses into a concrete reinforced with metal bars, the alkaline conditions of the solution within the pores are modified and the metal reinforcement loses the protection layer (de-passivation) [4]. A series of fundamental articles on the carbonation process are due to the author Papadakis [5,6,7,8,9]. Numerous works investigated the corrosion process of metallic reinforcement, one of the pioneering authors was Bazant [10]. The dependence of the cathodic reaction on the degree of water saturation was the subject of the work of Hue *et al.* [11], the kinetics of metal corrosion caused by carbonation were analysed in [12,13] and the coupling of oxygen transport with a micro-cell corrosion model also developed in [14]. Among others, reinforcement corrosion in a carbonated concrete has been simulated [15,16], corrosion in aluminium alloy modeled in Comsol Multiphysics® [17], the same mechanism induced by chloride ions studied in [18], while the transport of corrosive agents with electrochemical reaction system has been numerically represented by Ghods *et al.* [19]. On the other hand, microstructural reconstructions of the concrete using X-ray tomography are due to Lu *et al.* [20] and phase field computational methods describing the surface of a metallic anode to Mai and Soghrati [21]. Finally, several works have applied experimental and computational methods for modelling carbonation and corrosive phenomena, among others [22,23,24,25,26,27].

Computational model

Hypothesis of the model

The corrosive process can break the passivation layer protecting the steel, when the alkalinity of the aqueous solution (electrolyte) in the pores of the concrete decreases due to carbonation [4,10,28]. It consists of the dissolution of iron in the pore water, since Fe oxidizes and the Fe^{2+} ions pass into solution, according to the anodic reaction:

$$Fe \rightarrow Fe^{2+} + 2e^{-} \quad \text{(anode)} \qquad (1)$$

where e^{-} is the electron. The regions of the steel surface close to the anodic areas serve as cathodic sites and the e^{-} move towards them, creating an electrical current from cathodic to anodic regions. Simultaneously, atmospheric oxygen diffuses through the concrete towards the metal surface and, at the cathodic sites in contact with aqueous solution reacts with the electrons of reaction 1. The following reduction reaction originates with the formation of hydroxyl ions OH^{-}:

$$O_2 + 2H_2O + 4e^- \rightarrow 4OH^- \text{ (cathode)} \quad (2)$$

The electric current flows through the electrolyte, from the anodic surface to the cathodic area, caused by the transport in the opposite direction of the negative charges OH^-. On the other hand, the OH^- ions reaching the anodic region electrically neutralize the dissolved Fe^{2+} and form a solution of ferrous hydroxide $Fe(OH)_2$:

$$Fe^{2+} + 2OH^- \rightarrow Fe(HO)_2 \text{ (anode)} \quad (3)$$

The overall cell reaction, adding reactions 1, 2, and 3 is therefore:

$$2Fe + 2H_2O + O_2 \rightarrow 2Fe(HO)_2 \text{ (cell)} \quad (4)$$

Eqs. 2,3, and 4 show that O_2 is fundamental for the corrosive phenomenon of the reinforcement metal. In the pores, we assume that water is sufficient for developing the previous chemical reactions, influencing the corrosion process through two mechanisms [10]: a) the degree of saturation of the water affects the electrical resistivity of the concrete; b) the diffusion coefficient of the gases O_2 and CO_2 depends on the same degree of saturation.
Consequently, we establish the following hypotheses for the computational model:

a) concrete is a porous medium not completely saturated with water, where the carbonation phenomenon modifies the passivation state of the metallic reinforcement;
b) the oxidation-reduction process is modeled by oxidation of *Fe* and reduction of O_2 on the whole surface of the metallic bars (uniform corrosion by carbonation):
c) the atmospheric O_2 surrounding the concrete diffuses in the gas phase of the pores, towards the metal surfaces;
d) the electrochemical corrosion reactions are controlled by the O_2 concentration in proximity of the bars, with sufficient water;
e) the oxidized material of the reinforcement and its volumetric changes are neglected;
f) the corrosion phenomenon is modeled under steady-state conditions.

Physical model

Fig.1 illustrates the geometry of a reinforced sample [29], prepared with a Holcim MP/A-28 hydraulic cement, using the materials and relative quantities of Table 1. The final water/cement ratio is 0.57 with an aggregate/cement ratio of approximately 4.17. The upper side of Fig.1 gives a vertical view of the sample, with a 50 mm long exposed metal section belonging to a 110 mm high reinforcement bar. The extreme silicone coatings, insulating the other two sections of the bar are also indicated in this vertical view. The lower left side of Fig.1 provides a horizontal section with the position of a central bar and four outermost reinforcements, measured from the lateral surface of the cylindrical sample. The

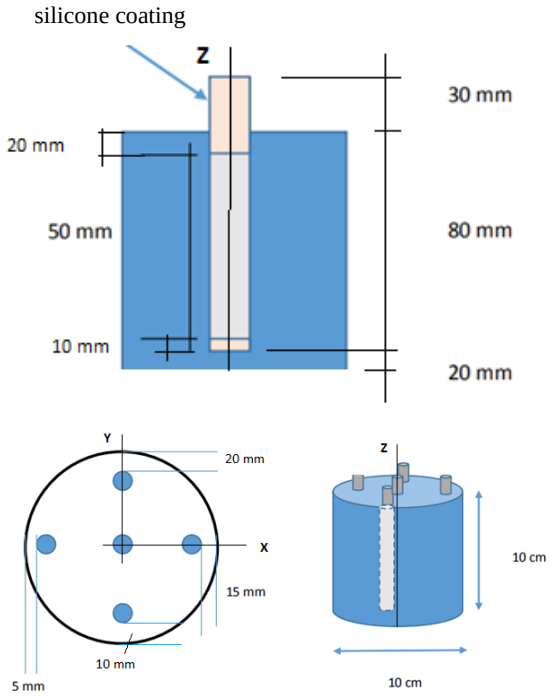

Figure 1. Schematic and dimensions of the reinforced concrete sample.

Table 1. *Composition of the concrete.*

Material	**Weight (kg)**
Hydraulic cement (MP/A-28)	381.927
Sand (wet)	687.31
Gravel (wet)	907.12
Water	197.45

Note: water to binder w/c ratio is 0.52, while the real value is 0.57, considering the humidity of the material.

rectangular Cartesian coordinate system, *x,y,z*, of the isothermal, steady-state, computational model is represented in the same Fig.1. We study the case of a sample carbonated for 33 days and exclude in the model the central bar, since it represents only a reference electrode.

Kinetics of the electrochemical reactions

A fundamental component of the computational model is the definition of the electrochemical reaction's kinetics on the electrode surfaces. First, using data based on an experimental process, the depths of the carbonation penetration is estimated for the concrete sample of Fig. 1 as a function of the carbonation time. For a sample carbonated 33 days in the accelerated chamber, at a CO_2 concentration of 25% and relative humidity of 65%, the penetration depth is 18 ± 1 mm from the outer cylindrical surface of the specimen. For a reinforced concrete sample carbonated 33 days, Table 2 gives the experimental values of the polarization test for four steel bars placed at different distance from the outer surface of the sample. As the carbonation is more intense, near the rods at 5 mm and 10 mm from the external surface, the corrosion potentials are more negative, and the current intensity is greater. For the bars at 15

Table 2. *Corrosion potential, current density, anodic and cathodic Tafel slopes of four reinforcement bars placed at different distances from the external cylinder surface.*

Distance: 5 mm			
Ecorr **(V)**	***icorr*** **(A/cm²)**	***ba*** **(V/dec)**	***bc*** **(V/dec)**
-0.6507	9.1468E-06	0.92964	-0.91109
Distance: 10 mm			
Ecorr **(V)**	***icorr*** **(A/cm²)**	***ba*** **(V/dec)**	***bc*** **(V/dec)**
-0.6051	7.5005E-06	0.88559	-0.82915
Distance: 15 mm			
Ecorr **(V)**	***icorr*** **(A/cm²)**	***ba*** **(V/dec)**	***bc*** **(V/dec)**
-0.5685	4.0430E-06	0.64922	-0.60148
Distance: 20 mm			
Ecorr **(V)**	***icorr*** **(A/cm²)**	***ba*** **(V/dec)**	***bc*** **(V/dec)**
-0.5239	6.4684E-06	1.0871	-0.8971

Note: the experimental values are measured by polarization resistance (the corrosion potential Ecorr is evaluated vs an Ag/AgCl saturated electrode at 25°C).

Table 3. *Exchange current density for iron oxidation and oxygen reduction of four reinforcement bars placed at different distances from the external cylinder surface.*

Distance: 5 mm	
i_O **(Fe oxidation) (A/cm²)**	i_O **(O_2 reduction) (A/cm²)**
0.1017 E-04	0.1308 E-06
Distance: 10 mm	
i_O **(Fe oxidation) (A/cm²)**	i_O **(O_2 reduction) (A/cm²)**
0.0744 E-04	0.0800 E-06
Distance: 15 mm	
i_O **(Fe oxidation) (A/cm²)**	i_O **(O_2 reduction) (A/cm²)**
0.0351 E-04	0.0089 E-06
Distance: 20 mm	
i_O **(Fe oxidation) (A/cm²)**	i_O **(O_2 reduction) (A/cm²)**
0.0541 E-04	0.1199 E-06

mm and 20 mm from the external surface the results are very similar to each other and show that the metal still maintains a certain degree of passivity.

Using the values of corrosion potential *Ecorr*, corrosion current density *icorr*, anodic *ba* and cathodic *bc* slopes of the Tafel curve, the anodic and cathodic exchange currents [28] of the metal bars can be estimated. The exchange current i_O for the oxidation of *Fe* is obtained by extrapolating the anodic Tafel curve towards the value of equilibrium potential of *Fe* (- 0.631 V vs *Ag/AgCl* electrode in 1M *KCl* solution at 25 °C). For the O_2 reduction, the exchange current is determined by extrapolating the cathodic curve towards the value of the O_2 equilibrium potential (1.007 V vs *Ag/AgCl* electrode in 1M *KCl* solution at 25 °C). Table 3 provides the values of i_O for oxidation and reduction mechanisms of the four steel bars. Next, the values of i_O , *ba*, and *bc* will be used in the model to describe the electrochemical kinetics of the metal/concrete interfaces.

Solution con Comsol Multiphysics®

In Comsol Multiphysics® 6.1 we define the electrochemical mechanisms of the reinforced concrete using the Second Current Distribution of the Corrosion Module [30]. The computation of the oxygen diffusion, gas required by the reduction reaction, is developed with the Transport of Dilute Species interface of the Chemical Reaction Engineering Module [31]. Using the Electrode Surface Coupling we introduce a flux boundary condition based on current densities and stoichiometric coefficient according to Faraday´s law.

For gaseous O_2, the concentration of 8.58 mol/m^3 is set at the boundaries, which corresponds to a partial volume of oxygen of 21% in the carbonation chamber. Except for the exposed metal surfaces, where reduction reactions take place, all other walls are considered impermeable to O_2. Using a correlation of Papadakis *et al.* [7], the porous medium is assigned a porosity of 0.32 and a water saturation equal to 0.27, for a water cement ratio of 0.57 and relative humidity of 65% in the carbonation chamber. It is assumed that O_2 moves in the gas phase of the pores with an effective transport coefficient of $2.5\text{x}10^{-8}$ m^2/s, as a function of porosity and relative humidity [7]. The initial O_2 concentration in the computational domain is also prescribed equal to 8.58 mol/m^3.

For the corrosion mechanism of the four reinforcing rods, concrete is modeled as an electrolytic medium with an effective electrical conductivity of 0.005 S/m [22]. Excluding the exposed areas of the metal, all other surfaces are required to be electrically insulated, both in the electrolyte and in the electrode. The calculation of the electric currents inside the metal is neglected since its electrical conductivity is much greater than that of the electrolyte.

Finally, the 3D computational mesh of finite element method generated in Comsol Multiphysics® is composed of $2.0\text{x}10^6$ tetrahedral elements and $1.2\text{x}10^5$ triangular elements, generating a steady-state model with approximately $8.55\text{x}10^5$ degrees of freedom.

Results and Discussion

For the corrosion of the metallic reinforcement, Fig. 2 shows the electric potential and current density lines of the electrolyte. When the electric current flows, the concrete (electrolyte) in the regions where the anodic reactions are more intense, presents a more positive electrical potential than the concrete

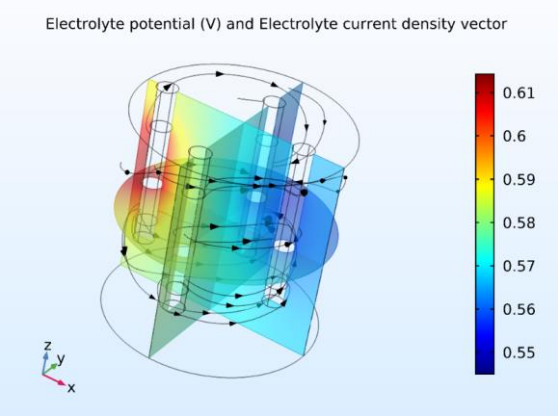

Figure 2. Electric potential and current density vector in the electrolyte.

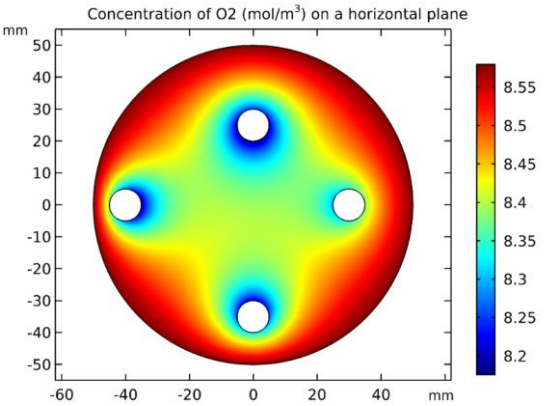

Figure 3. O_2 concentration on a horizontal plane of the reinforced concrete (z=50 mm).

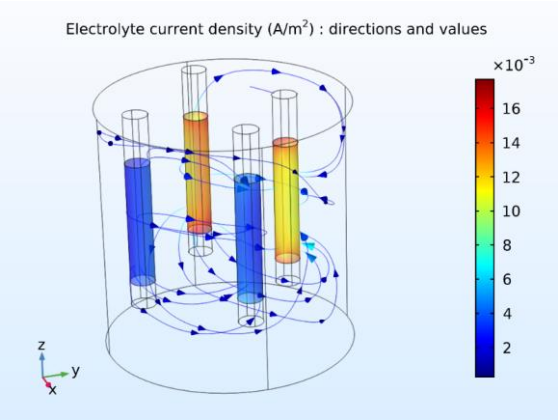

Figure 4. Current density lines in the electrolyte and values on the bar's surfaces.

of the regions where these are less intense. Therefore, when *Fe* is oxidized, the Fe^{++} ions dissolve in the nearby concrete, while the e^- move in the metal and, close to the cathodic region, are available for the reduction of O_2. In Fig. 2 the electric current density in the electrolyte is directly proportional to the electric potential difference (Ohm's law). This quantity is given by the difference between the potential of the electrolyte close to the most intense anodic regions, minus the potential of the electrolyte of those regions where the corrosive phenomenon is less strong. Fig. 3 plots the O_2

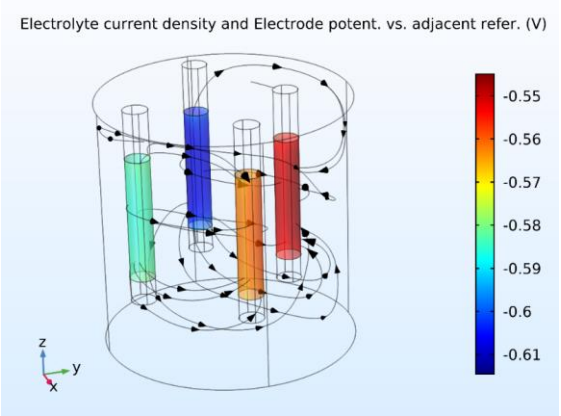

Figure 5. Current density lines in the electrolyte and electrode potential vs reference.

distribution in a horizontal plane that cuts the cylinder at half its height (z =50 mm), intersecting the metallic rods. The decrease in O_2 is evident in the area near the metal, particularly in the regions facing the centre of the cylinder. This is due to the consumption of O_2 in the reduction reactions, representing a sink modeled by the Faraday´s law. The current density lines in the electrolyte volume are given in Fig. 4, where we observe that in proximity to the bar positioned 5 mm from the outer surface on the negative side of the *x* axis, the electric current is more intense and the O_2 concentration is low, due to the reduction reactions. For the reinforcement placed 20 mm from the exterior wall on the positive side of *y* axis, the O_2 is even lower, since this electrode is more distant from the periphery, where the boundary concentration is fixed. In the model, which implements the electrochemical kinetics of the Tafel equations and neglects the calculation of the electric current inside the metal, the potential ϕ_s of the metallic phase is defined as null and the overpotential η is computed as $\eta = \phi_s - \phi_l - E_{eq} = -\phi_l - E_{eq}$, where E_{eq} is the equilibrium potential and ϕ_l is the electrolyte potential. Fig. 5 depicts the current density lines in the electrolyte and the electrical potential of the electrode *vs.* the reference. The electrolyte current density lines arise in the regions where *Fe* oxidation is most intense, *i.e.* in the outermost rods of the carbonated concrete. The mechanism is highlighted in Fig. 6 by plotting the electrolyte potential and the current density in a horizontal plane at z = 50 mm. We observe that the areas with the highest potential are located near the outermost oxidized bars. Fig 7 gives the magnitude of the current density in the electrolyte, on the horizontal surface z =50 mm. For all metal bars, the graph of Fig. 8 plots the oxidation (or corrosion) current density of *Fe*, computed along a vertical edge opposite the center of the concrete specimen and facing outwards. On the other hand, Fig. 9 provides the computational results of the O_2 reduction corresponding to the same edge. Fig. 8 points out that the *Fe* oxidation current for the rod 5 mm from the outer surface is greater than those of the rest, since it is located inside a carbonated area

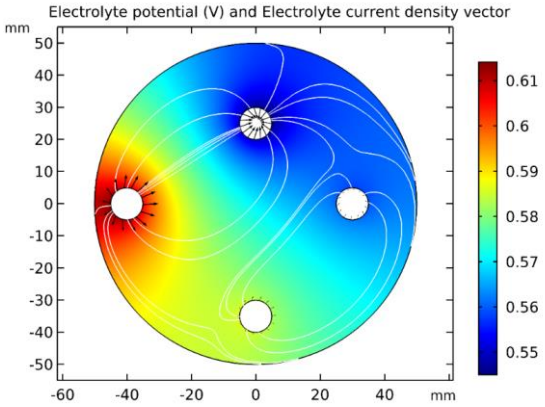

Figure 6. Electric potential and electrolyte current density vector on a horizontal plane (z=50 mm) of the reinforced concrete.

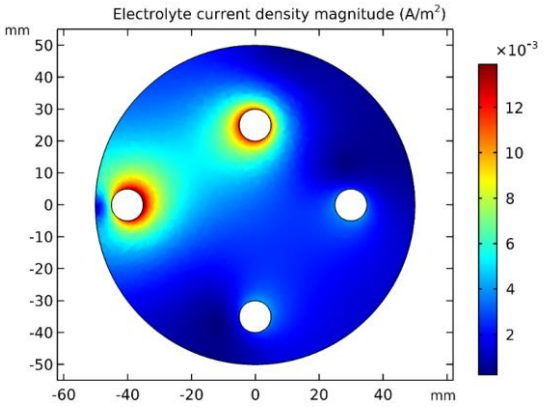

Figure 7. Electrolyte current density magnitude on a horizontal plane (z=50 mm) of the reinforced concrete.

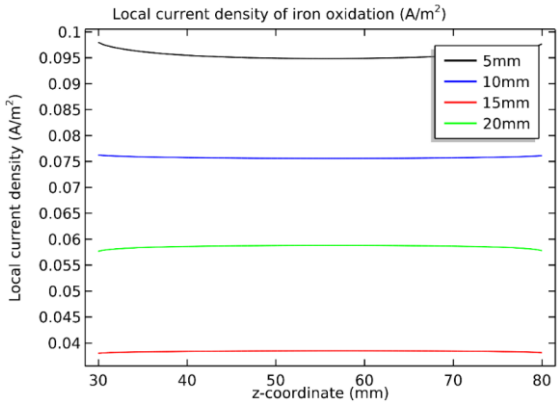

Figure 8. Local current density of iron oxidation on the electrode interface, for the 4 bars placed at different positions in the reinforced concrete.

where the electrochemical corrosion mechanism is more favourable. According to Table 3, the bars, except the reinforcement placed 20 mm from the outside, are characterized by a corrosion current decreasing with the distance from the periphery. The numerical results of Fig. 9 show a similar behaviour for the O_2 reduction, *i.e.* the reduction current density is greater for the outermost reinforcement, where the O_2 also diffuses more rapidly from the environment. For the more external bars, located respectively at 5 mm and 10 mm, the values of the anodic current densities are higher than those of the corresponding cathodic currents. These results are analysed with the interface potential, namely with the anodic overpotential η. When in some regions the ϕ_l potential is lower, there η is higher and thus the corrosion current given by the Tafel oxidation equation. In the case of O_2, the reduction rate increases with its concentration in the electrolyte, and, by the Tafel cathodic equation, with the most negative values of η corresponding to the interfaces placed in areas where the ϕ_l potential is greater.

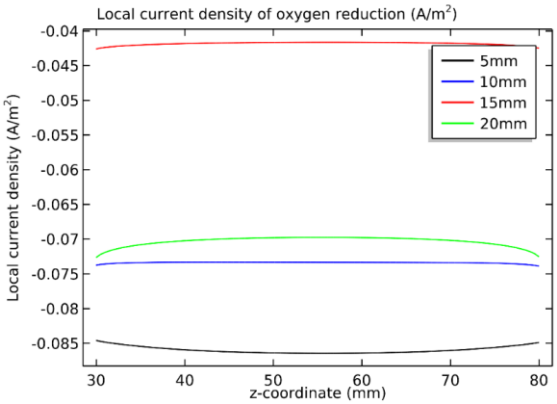

Figure 9. Local current density of oxygen reduction on the electrode interface, for the 4 bars placed at different positions in the reinforced concrete.

Conclusions

Using Comsol Multiphysics® 6.1, we have developed a model of reinforcement bars corrosion by incorporating experimental kinetic data to reflect a carbonation mechanism interesting the concrete. Starting from experimental values of corrosion potential, corrosion current density, anodic, and cathodic slopes of the Tafel curve, the values of exchange currents have been computed and then used to simulate the corrosion of four reinforcing bars. The analysis of the computational results has shown that when the carbonation is more intense, as occurs with the outermost bars, the corrosion potential is more negative, and the current density presents larger values. According to these results, the external bars are characterized by stronger corrosion and reduction currents, phenomena depending also on the oxygen concentration values associated to the gas diffusion, process which has been coupled to the corrosion mechanism.

References

[1] ASCE, "Report card for America's infrastructure", American Society of Civil Engineers, Reston, VA, 2013.

[2] X. Wang, M. Nguyen, M. Stewart, M. Syme and A. Leitch, "Analysis of climate change impacts on the deterioration of concrete infrastructure". *Part 1: Mechanisms, Practices, Modeling and Simulations - A Review*, CSIRO, Canberra, 2010.

[3] W. Hayden, W.G. Moffatt and J. Wulff, "*The structure and properties of materials*", Vol. III Mechanical Behavior, John Wiley and Sons, New York, 1965.

[4] K. Tuutti, "*Corrosion of steel in concrete*", Swedish Cement and Concrete Institute RIT-Stockholm, 1982.

[5] V.G. Papadakis, C.G. Vayenas and M.N. Fardis, "A reaction engineering approach to the problem of concrete carbonation", *American Inst. of Chemical Engineers*, 35, N.10, 1639-1650, 1989.

[6] V.G. Papadakis, C.G. Vayenas and M.N. Fardis, "Experimental investigation and mathematical modeling of the concrete carbonation problem", *Chemical Engineering Science*, 46, N.5/6, 1333-1338, 1991.

[7] V.G. Papadakis, C.G Vayenas and M.N. Fardis, "Physical and chemical characteristics affecting the durability of concrete", *ACI Materials Journal*, 88, N.2, 186-196, 1991.

[8] V.G. Papadakis, M.N. Fardis and C.G. Vayenas, "Hydration and carbonation of pozzolanic cement", *ACI Materials Journal*, 89, N.2, 119-130, 1992.

[9] V.G. Papadakis, M.N. Fardis and C.G. Vayenas, "Effect of composition, environmental factors and cement-lime mortar coating on concrete carbonation", *Materials and Structures*, 25, 293-304, 1992.

[10] Z.P. Bazant, "Physical model for steel corrosion in concrete sea structures", *Journal of the structural division-Proceedings of the ASCE*, 105, n. ST6, 1137-1153, June 1979.

[11] B. Huet, V. L'Hostis, G. Santarini, D. Feron and H. Idrissi, "Steel corrosion in concrete: deterministic modeling of cathodic reaction as a function of water saturation degree", *Corrosion Science*, 49, 1918-1932, 2007.

[12] P. Dangla and W. Wridi, "Rebar corrosion in carbonated concrete exposed to variable humidity conditions. Interpretation of Tuutti's curve", *Corrosion Science*, 51, 1747-1756, 2009.

[13] M.G. Sohail, "Corrosion of steel in concrete: Development of an accelerated test by carbonation and galvanic coupling", *PhD thesis, Université de Toulouse*, 2013.

[14] R.R. Hussain and T. Ishida, "Development of numerical model for FEM computation of oxygen transport through porous media coupled with micro-cell corrosion model of steel in concrete structure", *Computers and Structures*, 88, 639-647, 2010.

[15] T.T.H. Nguyen, B. Bary and T. de Larrard, "Coupled carbonation-rust formation-damage modeling and simulation of steel corrosion in 3D mesoscale reinforced concrete", *Cement and Concrete Research*, 74, 95-107, 2015.

[16] R.A. Robayo-Salazar, A.M. Aguirre-Guerrero and R. Mejia de Gutierrez, "Carbonation-induced corrosion of alkali-activated binary concrete based on natural volcanic pozzolan", *Construction and Building Materials*, 232, 117189, 2020.

[17] N. Murer, N. Missert and R. Buchheit, "Towards the modeling of microgalvanic corrosion in aluminum alloys: the choice of boundary conditions", *Proceedings of the Comsol Users Conference*, Boston (USA), 2008.

[18] C.Y. Kim and J.K Kim, "Numerical analysis of localized steel corrosion in concrete", *Construction and Building Materials*, 22, 1129-1136, 2018.

[19] P. Ghods, K. Karadakis, O.B. Isgor and G. McRae, "Modeling the chloride-induced corrosion initiation of steel rebar in concrete", *Proceedings of the Comsol Conference 2009 Boston*, Boston, Ma, 2009.

[20] Y. Lu, E. Garboczi, D. Bentz and J. Davis, "Modeling the chloride transport in cracked concrete: a 3D image-based microstructure simulation", *Proceedings of the Comsol Conference 2012 Boston*, Boston, Ma, 2012.

[21] W. Mai and S. Soghrati, " New phase field model for simulating galvanic and pitting corrosion processes", *Electrochimica Acta*, 260, 290-304, 2018.

[22] C. Cao, "3D simulation of localized steel corrosion in chloride contaminated reinforced concrete", *Construction and Building Materials*, 72, 434-443,2014.

[23] N. Seigneur, E. Kangni-Foli, V. Lagneau, A. Dauzeres, S. Poyet, P. Le Bescop, E. L'Hopital and J.B. d'Espinose de Lacaillerie, "Predicting the atmospheric carbonation of cementitious materials using fully coupled two-phase reactive transport modelling", *Cement and Concrete Research*, 130, 105966, 2020.

[24] P. Liu, Z. Yu and Y. Chen, "Carbonation depth model and carbonated acceleration rate of concrete under different environment", *Cement and Concrete Composites*, 114, 103736, 2020.

[25] K. Mei, Z. He, B. Yi, X. Lin, J. Wang, H. Wang and J. Liu, "Study on electrochemical characteristics of reinforced concrete corrosion under the action of carbonation and chloride", *Case Studies in Construction Materials*, 17, e01351, 2022.

[26] R.A. Robayo-Salazar, A.M. Aguirre-Guerrero and R. Mejia de Gutierrez, Carbonation-induced corrosion of alkali-activated binary

concrete based on natural volcanic pozzolan, *Construction and Building Materials*, 232, 117189, 2020.

[27] C. Wei, C.S. Wojnar and C. Wu, Hydro-chemo-mechanical phase field formulation for corrosion induced cracking in reinforced concrete, *Cement and Concrete Research*, 144, 106404, 2021.

[28] D.A. Jones, "*Principles and prevention of corrosion*", 2nd Ed., Macmillian Publishing Company, New York, 1992.

[29] B. Chiné, R. Jimenez and R. Cuevas, "Corrosión del concreto reforzado y DEgradación de sus propiedades MECánicas (CODE_MEC2): Etapa 2 Estudio experimental y modelación computacional de la carbonatación y corrosión del concreto reforzado", código 1490020, *Informe Final*, *Dirección de Proyectos VIE*, *ITCR*, 2021.

[30] Comsol AB, *Corrosion Module*, User's Guide, Version 6.1, 2022.

[31] Comsol AB, *Chemical Reaction Engineering Module*, User's Guide, Version 6.1, 2022.

Acknowledgements

The authors gratefully acknowledge the financial aid provided by the Vicerrectoría de Investigación y Extensión of the Instituto Tecnológico de Costa Rica, through the project 5401-1411-3001.